Article
Vol. 25, No. 3, p. 321–331, June 2021
https://doi.org/10.1007/s12303-020-0024-9
pISSN 1226-4806 eISSN 1598-7477
Geosciences Journal GJ

Integrated interpretation of geophysical data from Zagros mountain belt (Iran)

Mansoure Montahaei[1]*, Pilar Queralt[2], Juanjo Ledo[2], Behrooz Oskooi[1], Josep A. Muñoz[2], and Alex Marcuello[2]

[1]Institute of Geophysics, University of Tehran, End of Amirabad e Shomali Ave., PO Box 14155-6466, Tehran, Iran
[2]Institut de Recerca Geomodels, Departament de Dinàmica de la Terra i de l'Oceà, Facultad de Ciencias de la Tierra, Universitat de Barcelona, Martí i Franqués, s/n 08028, Barcelona, Spain

ABSTRACT: Fluid composition and distribution, the key factors determining geoelectric structure in a seismically active region, are controlled by local and regional stresses and rheological contrasts. Two closely located magnetotelluric and seismic velocity profiles are jointly interpreted to recover more accurately the structural boundaries and fluid distribution within the crust in the central Zagros collision zone, one of the world's most seismically active mountain belt. A multi-site and multi-frequency approach was used for the strike analysis of regional structure and decomposition of distortion effects on magnetotelluric data. Distortion corrected magnetotelluric data were then used for two-dimensional inversion modeling. The results indicate distinct conductive structures within the crust: (i) a thick conductive overburden in the southwest of the profile, (ii) high conductivities attributed to the fault zone conductors (FZCs) and (iii) an almost concave conductor extending from middle to lower crust in the central–eastern portion of the mountain belt, beneath the High Zagros (HZ). Comparison with the already available S-wave velocity structure, obtained by joint inversion of P-wave receiver functions and surface wave dispersion data shows that these main conductive features are spatially correlated with a low-velocity layer representative of the sedimentary cover overlying the Arabian platform and a velocity contrast bounded by the main Zagros thrust (MZT) fault, indicating the presence of fault zone fluids. The joint interpretation of magnetotelluric inverse modeling and seismicity data also shed light on fluid generation influencing rock deformation and seismicity in this region. It suggests that beneath the HZ, deep crustal fluids generated through metamorphism may promote aseismic deformations before high stresses are builtup and cause the north-eastern part of the Zagros Fold and Thrust Belt (ZFTB) to be seismically inactive compared to its south-western part.

Key words: Zagros, magnetotellurics, resistivity, seismicity, fluids

Manuscript received October 23, 2019; Manuscript accepted April 28, 2020

1. INTRODUCTION

The Zagros orogen is a key structural element of the Alpine–Himalayan belt. The range represents the surface exposure of the Arabian-Eurasian collision, known as an example of a young collision system. It accommodates spectacular, world-renowned whaleback folds, hosting vast petroleum reserves. It is amongst the most rapidly deforming and seismically active fold and thrust belts and proved to be an ideal setting in which to investigate competing models of the fold and thrust deformation (Nissen et al., 2011). Studying the deep crustal structure of the Zagros belt could thus provide a better understanding of the dynamic earth processes in a continental collision.

Most of the structural studies are based on the measurements of surface geology and instrumental earthquake records. Earlier studies suggest that larger earthquakes occurred in the Zagros basement (Talebian and Jackson, 2004). Recent studies of earthquake faulting based on radar interferometry show a depth distribution of coseismic faulting; while the moderate size (5–6 M_W) earthquakes ruptured the competent group of mechanically strong strata in

*Corresponding author:
Mansoure Montahaei
Institute of Geophysics, University of Tehran, End of Amirabad e Shomali Ave., PO Box 14155-6466, Tehran, Iran
Tel: +98-21-88001115, Fax: +98-21-88009560, E-mail: mmontaha@ut.ac.ir

Electronic supplementary material
The online version of this article (https://doi.org/10.1007/s12303-020-0024-9) contains supplementary material, which is available to authorized users.

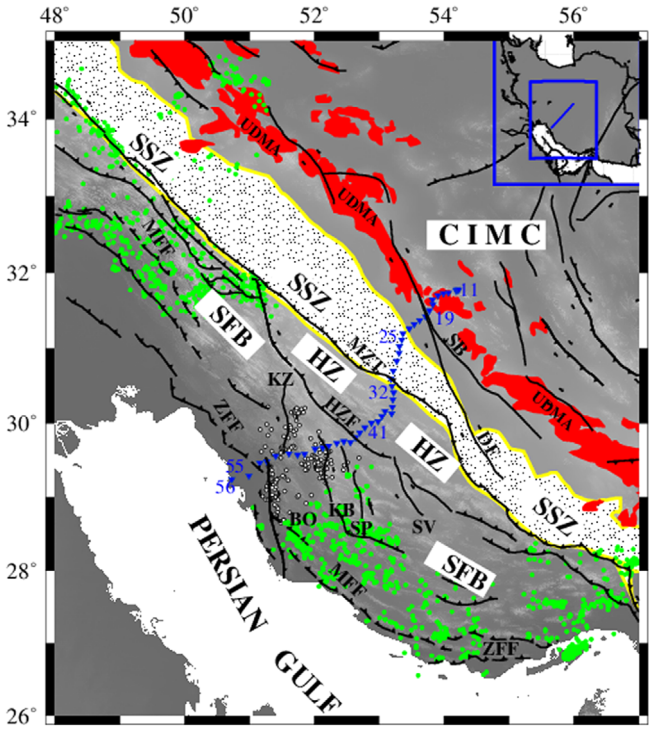

Fig. 1. Geological map of the Zagros mountain belt showing the location of MT sites (blue inverse triangles). Also shown are the main structural units (Simply Folded Belt (SFB), High Zagros (HZ) and Central Iran Micro Continent (CIMC)) and the major faults (black lines, dashed if blind): BO, Borazjan Fault; DEF, Dezful Embayment Fault; KZF, Kazerun Fault; MFF, main front fault; HZF, High Zagros Fault; MZT, Main Zagros Thrust Fault; SV, Sarvestan Fault; SP, SabzPushan Fault; SU, Surmeh Fault; ZFF, Zagros Foredeep Fault; DF, Dehshir Fault; SB, Shahr e Babak fault. The yellow solid line delineates the border of Sanandaj–Sirjan zone (SSZ). White and green dots are epicentres from GCCEL database with magnitudes between (2.5–7) M_W (Karasozen et al., 2019), the white ones are projected in the 2D MT resistivity model. The inset shows the location of the regional map.

the lower sedimentary cover (at depths of 5–10 km), their microseismic aftershocks are vertically separated and occurred within the basement at depths of ~10–20 km. Coulomb stress changes, the effects of loading or shaking and dynamic stress transfer caused by shaking are possible scenarios lead to the separation (Nissen et al., 2011).

Nevertheless, very few geophysical investigations have been conducted to constrain the deep crustal structure of the Zagros. To improve our knowledge about the crustal structure of Zagros collision zone, we analyze broadband magnetotelluric (MT) data, recorded at 46 stations along a 470 km profile, crossing the main morpho-tectonic units in this region (Fig. 1). It starts near Busher on the northern coast of Persian Gulf, crosses the ZFTB, where a high level of seismicity is accommodated with earthquakes magnitudes smaller than seven and hypocenters concentrated at a depth between 8–15 km. To the NE the profile further crosses the Precambrian metamorphic rocks of Sanandaj Sirjan Zone (SSZ), bounded by the Urumieh-Dokhtar magmatic assemblages (UDMA) produced by the Eiocen to present time volcanic activities. The profile ends near Yazd, in the SW of central Iran microcontinent (CIMC) block.

The data were preliminary interpreted by 2D inverse modeling (Oskooi et al., 2013) and further investigated by sensitivity analysis of the inversion results (Layegh-Haghighi et al., 2018). This paper extends our previous findings by removing distortion effects from MT data to obtain a new and more accurate 2D resistivity model. In the next stage, we jointly interpret inversion results with the recent seismicity data and the latest seismic velocity models (Motaghi et al., 2015; Karasözen et al., 2019). Joint interpretation of seismic velocity and electrical resistivity models allows to better constraint geological scenarios (Gabàs et al., 2016; García-Yeguas et al., 2017).

2. GEOLOGICAL SETTING AND GEOPHYSICAL BACKGROUND

Subsequent to the closure of the Neothetys ocean and its subduction beneath Iranian microplate during Mesozoic and early Cenozoic, the deformed north-eastern edge of the Arabian plate collided obliquely with central Iran continental block. Zagros mountain belt was formed as the surface exposure of this collision. Magneto-stratigraphy and strontium isotope stratigraphy of the foreland basin sedimentation restrict the initial stage of mountain building at 27 ± 2 Ma (Pirouz et al., 2017). The estimates of underthrust Arabian lithosphere (≈ 350 km) and the average shortening rate across the Zagros (ca. 13.5 mm/yr) imply that almost half of the convergence between Arabia and Eurasia is manifested by the crustal thickening across the Zagros and the remained shortening is due to the thrusting and eclogtization of the Arabian crust (Masson et al., 2005; Paul et al., 2010; Pirouz et al., 2017).

Based on topography, exposed stratigraphy and seismicity, the High Zagros fault (HZF) divides the ZFTB into two distinct zones: the Simply Folded Belt (SFB) in the southwest and the High Zagros (HZ) in the northeast. While the topography is lower than 1500 m throughout the SFB with rare exposes of Paleozoic strata, the topography averages 1500–2000 m and the stratigraphy exposes Paleozoic and Mesozoic levels in the High Zagros (Nissen et al., 2011).

There is no basement outcrop in the Zagros, however different estimates of the total sedimentary cover show its thickness varies from ~14 km in the northwest of SFB to ~10 km in the far southeastern of SFB. To the northeast, into the HZ, it decreases to lower values due to the erosion (Sherkati et al., 2006). Furthermore, a recent inverse modeling of potential field data shows high density contrasts of the embedded units among active faults in this region (BF, KZF, MFF, and HZF faults), which represent

basement rocks uplifted close to the surface (Abedi et al., 2018).

Geological complexities make control-source seismic imaging of Moho depth variation impossible. However, most of our knowledge about crustal and lithospheric upper mantle structure comes from seismology and non-seismic geophysical data (Paul et al., 2010).

The first coarse map of Moho depth variation beneath the Zagros Orogeny, provided by the modeling of the Bouguer anomaly data, showed crustal thickening from 40 km beneath the Persian Gulf to 65 km beneath the MZT (Dehghani and Makris, 1984; Snyder and Barazangi, 1986). However, receiver function analysis of teleseismic earthquake details showed that crustal thickness is 42 ± 2 km beneath the ZFTB. From 30 km SW of the MZT, crustal thickness increases on a 170 km length and reaches a maximum value of 69 ± 2 km beneath the low elevation of SSZ (and not beneath the High Zagros) between 50 and 90 km NE of the MZT. The MOHO depth decreases to its average value around 45 km, beneath CIMC (Paul et al., 2006). These values are consistent with the crustal thicknesses obtained from 1D absolute S-velocity model beneath each station (Motaghi et al., 2015) and also the depth section of S-wave receiver functions (SRFs, Motaghi et al., 2017).

Lithosphere is thick beneath the Zagros (thicker than 240 km) and becomes relatively thinner (130 ± 15 km) beneath CIMC (Motaghi et al., 2015).

Upper mantle structure and mantle transition zones, based on the PRF migrated depth section down to 800 km depth (Motaghi et al., 2017), show: (i) an intra lithospheric mantle decoupling, which lets on differential buckling and introduces a deforming viscose layer representative of the lid rheological parameters, (ii) lithospheric scale accommodation of the south Zagros contract, (iii) minor thrusting of lithospheric mantle beneath central Iran, indicating that Zagros collision is in its initial stage and (iv) a low dip slab subduction coincident with the slab stagnation close to the transition zone (Manaman et al., 2011).

3. MAGNETOTELLURIC DATA ANALYSIS AND INVERSION

The MT method is a passive electromagnetic exploration technique which records naturally varying horizontal electric and magnetic fields as well as the vertical component of the magnetic field. MT transfer functions are calculated at different frequencies of each station from the impedance tensor, which linearly relates horizontal electric and magnetic field components in the horizontal plane and also the ratio of horizontal to vertical magnetic field components, known as tipper vectors. The magnitude (scaled as apparent resistivity) and phase of impedance tensor elements are commonly used for MT data presentation. Penetration depths of EM fields depend on their frequencies (increase with decreasing frequency) as well as the electrical conductivity of the subsurface and provide depth sounding estimates of the MT transfer functions. In 2D earth situations, where electrical resistivity is constant along one of the horizontal direction (geoelectrical strike direction of the regional structure) EM fields are decomposed into two distinct modes; transverse electric (TE) and transverse magnetic (TM) modes (Chave and Jones, 2012). The MT method allows unraveling the electrical resistivity of the subsurface at lithospheric scales and define complex structure and tectonic history of collision zones (Unsworth, 2010 and the case studies therein).

The phase tensor method (Caldwell et al., 2004) was employed to determine the dimensionality of the data. A map of phase tensor ellipses at the different periods of all sites is presented in Figure 2. For most sites at short periods, where EM fields have small penetration depths, they are circles, characteristic of 1D regional geoelectric structure at these depths. Increasing the period, penetration depths get larger and the phase tensors delineate ellipses whose major and minor axes are parallel or perpendicular to the N45°W direction. An investigation of rose histograms of phase tensor ellipse axis direction confirmed a regional geoelectric strike angle of N45°W at long periods (> 1 second) for the majority of sites along with the profile (Fig. S1 in the electronic supplementary material). Considering the 90° ambiguity inherent in the method, this direction is coincident with the general trend of the ZFTB, as the main geologic structure in this region. Furthermore, the face color of the phase tensors is determined by the β skew angle, a distortion free measure of asymmetric properties introduced in the data by 3D structures. The accepted value of this parameter above which the structure could not be considered as 2D is 5°. The small β skew angles calculated at

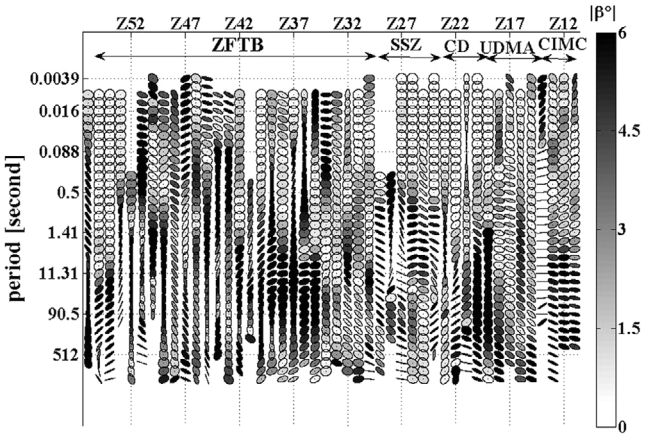

Fig. 2. The phase tensor ellipse map showing the dimensionality for the Zagros profile. The major and minor axes of the ellipses correspond to the strike direction of regional geoelectric structure. The brightness and contrast of the ellipses express the β skew angle, which is a measure of asymmetry produced by 3-D structures.

https://doi.org/10.1007/s12303-020-0024-9

most periods for all sites implement that a 2D inverse modeling strategy is acceptable for this data set.

Once the dimensionality was determined we applied the Groom and Bailey (GB) decomposition method following the multi-site, multi-frequency methodology of McNeice and Jones (2001), to correct MT data for galvanic distortion parameters. The low values of least square misfits between distortion model responses and the observed data (Figs. S2 and S3 in the electronic supplementary material), calculated at most periods of all sites, indicate that the proposed distortion model of local 3D inhomogeneities superimposed on a regional 2D structure striking in an approximate N45°W direction, appropriately resembles the MT dataset. Note that the results of this procedure are the most accurate regional 2D impedances determined in a given coordinate system and are not the same as those obtained by just rotating data into that coordinate system (the strategy used in the previous modeling of this data set (Oskooi et al., 2013; Layegh-Haghighi et al., 2018). A comparison between measured data after a simple rotation into strike direction (applied in previous modelings of the dataset) and after decomposition into the strike direction (applied in present work) is provided in the electronic supplementary material (Fig. S4).

Distortion corrected TE and TM mode responses of regional structure recalculated by the GB decomposition approach are then modeled throughout the regularized inversion algorithm suggested by Rodi and Mackie (2001). The algorithm is implemented in the Geosystem's WinGLink interpretation software and employs a non-linear conjugate gradient (NLCG) method to minimize a penalty function composed of least-square measure of data misfit (Φ_d) and squared Laplacian of the horizontal and vertical resistivity gradients representative of model roughness (Φ_m). The contribution of each datum (d_i^{obs}) is weighted with respect to its error (σ_i) and a specified relative error floor (ε). The Lagrange multiplier (τ) is a trade-off parameter, controlling the relative weight given to the data fit and model roughness:

$$E(m) = \Phi_d + \tau\Phi_m, \quad (1)$$

where $\Phi_d = \sum_i \left(\frac{d_i^{obs} - d_i^{cal}}{\max(\sigma_i, \varepsilon d_i^{obs})} \right)^2$, and $\Phi_m = \int \left| \nabla^2 (\vec{m} - \vec{m}_0) \right|^2 dA$.

TM mode impedances expanding over six period band decades, between 0.0039–1448 seconds, have been considered for the inversion. However, in order to avoid intermediate-scale three-dimensional effects that substantially can distort the TE mode responses (Ledo, 2005), their maximum period was restricted to 10 s for the first 30 iterations and 100 s for the remaining. Inaccurate data points with large error bars and those representing random scattering were removed before the inversion. Furthermore, the D^+ consistency assessment (Parker, 1982) was performed where essential and inconsistent data points were excluded from the inversion procedure. Data errors have been used; otherwise the errors of the apparent resistivities and phases were set to 10% and 5% (equivalent to 1.45°), respectively.

Three-dimensional numerical experiments have shown that the TM mode impedances are more robust to along strike structural changes (Ledo et al., 2002; Ledo, 2005; Wannamaker et al., 2009). In addition, electric currents associated with the TM mode electromagnetic fields flow across geoelectrical strike and enhance the resolution of large-scale conductive fault structure. Accordingly, the TM mode impedances were emphasized through the model construction. The inversion runs initiated from a homogeneous half space as the starting model, where the Persian Gulf was the only feature fixed in order to model accurately the effects of the conductive sea water.

We used some steps to produce a final inversion model. Error floors were introduced to control the weighting of each data type (data with smaller error dominate the Φ_d in Eq. 1). In order to initiate the inversion model based on TM mode phase data, the error floors were 50% for apparent resistivity and 1.45° for phases in TM mode data. In the following numerical experiments, the error floor of TM resistivities reduced to 10% and TE phases and resistivities incorporated through the procedure, sequentially. The error floors of the final inversion run were 1.45° for phases and 10% and 25% for TM and TE apparent resistivities, respectively.

Different data composition including TE, TM and bimodal data were examined through inverse modeling (results are presented in the electronic supplementary material, Figs. S5 and S6). The fit of model responses with the measured data are presented as the normalized data misfit for all stations along the profile (Fig. S7 in the electronic supplementary material) and pseudo sections of measured data and model responses in the electronic supplementary material (Figs. S8 and S9). While the RMS is less than 4 for the TE and TM modes, but the TM mode responses provide a better fit with the measured data, in terms of the global RMS misfit criterion (Fig. S7).

4. DISCUSSION

4.1. Regional Geoelectric Structure

The results of bimodal MT data inversion (Fig. 3) will be argued in the following. The Arabian crust is more conductive and heterogeneous than Eurasia. Fixing the Persian Gulf as a conductive body in the starting model, a resistive structure (R1) is recovered beneath the southwest end of the profile, resembling the downgoing Arabian plate. It was absent in the previous inversion results of the data (Oskooi et al., 2013; Layegh-Haghighi et al., 2018). To the southwest of the Kazerun fault, the resistivity

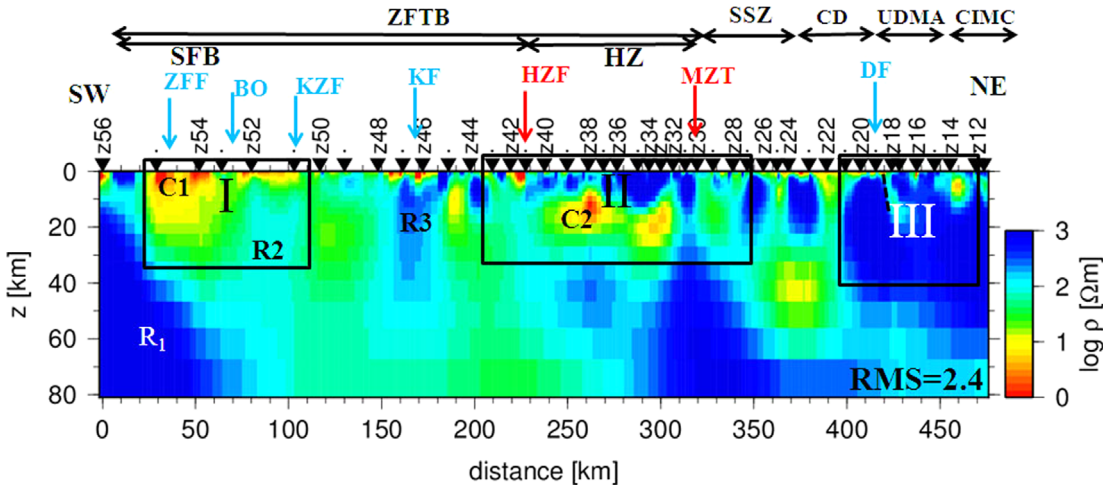

Fig. 3. Non-linear 2-D inversion model of electrical resistivity beneath the Zagros profile obtained for joint TE and TM modes of the impedance tensor (a vertical exaggeration of 1.5:1 is used). Arabian plate below the SW of the profile is dipping NE ward, beneath Central Iran. Major faults are labeled as in Figure 1 (red: SW-NE striking faults, blue: N-S striking faults). Rectangles I, II, III represent spatial partitioning of the zones with high velocity/resistivity correlation outlined in Figure 6 (zones I, II and III). Different grid sizes used in the seismic and MT models result in large coverage gaps.

model shows for the uppermost part of the crust, a thick conductive layer (C1) from the surface to a depth of about 15 km, underlain by the Pre-Cambrian crystalline basement of Arabia. Two resistive bodies (R_2, R_3) are imaged coincident with the surface traces of right-lateral strike-slip faults: Kazerun and Karebas faults. They are major basement faults which dragged and displaced anticline axes by at least 10 km (Khadivi, 2010). A prominent conductive feature on the MT image appears at the crustal depths in the middle part of the profile (C2), underneath the High Zagros. The surface trace of the MZT coincides with the sharp conductivity contrast at the eastern edge of this feature. A thin near-surface conductive layer, representing massive Neogene sediments of Central Iran is also imaged in the upper crust, beneath the NE part of the profile.

The maximum smoothness constraint used in the MT inversion algorithm to find a unique inverse model tends to smear the conductor to unrealistically great depths. Furthermore, MT data are most sensitive to the conductance (the product of the layer thickness and conductivity) of the subsurface and different models with constant conductance but dissimilar thicknesses and conductivities can fit equally well a given set of MT data. The solution is the constrained inversion where the bottom of its starting model is fixed at a high value of 1000 Ωm. Then by moving upward the top of the resistive half-space until model responses could not fit the data properly, one could find the shallowest depth of the conductor's bottom, permitted by the data (Li et al., 2003). We applied this strategy and found that the conductive layer beneath the southwest of the profile is at least extended deeper than 10 km depth (Fig. S10 in the electronic supplementary material).

Comparison with previous modeling results (Oskooi et al., 2013; Layegh-Haghighi et al., 2018) shows major conductive anomalies recovered at similar locations beneath the profile (Fig. S11 in the electronic supplementary material), but their spatial extent is much more restricted on the resistivity cross-section represented in Figure 3, implying the fact that the MT data have been corrected by GB decomposition prior to modeling. There are also some inconsistencies at regions where phase tensors show erratic behavior and large β skew angles.

4.2. Origin of High Conductivity in Central Zagros

A significant property of the model presented in Figure 3 is the very high conductance (up to 6000 S, which would correspond to the conductance of a two-kilometer-thick layer of seawater) recovered in the upper crust with a generally decreasing trend from SW to the NE along with the profile (Fig. S12 in the electronic supplementary material). The best explanation for such a high electrical conductance is saline fluids (reported in the eastern Zagros (Bosak et al., 1998)) filling the fractures and giving rise to the high electrical conductivity. Meteoric waters transported towards the fault zone by topography and/ or fluids circulating in the damage zone of a fault system characterize the upper few kilometers of the crust within a fault as a conductive zone, known as a fault zone conductor (FZC), (Ritter et al., 2005). The width and depth extent of the FZCs vary along the Zagros profile (e.g., confined conductive zones centered on the KF and HZF faults and weakly revealed conductivity at DF fault in Fig. 3). A distinct lack of FZC is observed beneath the MZT, implying that an FZC is not required to fit the data.

To further examine the potential role of fluids at the FZCs, we

https://doi.org/10.1007/s12303-020-0024-9

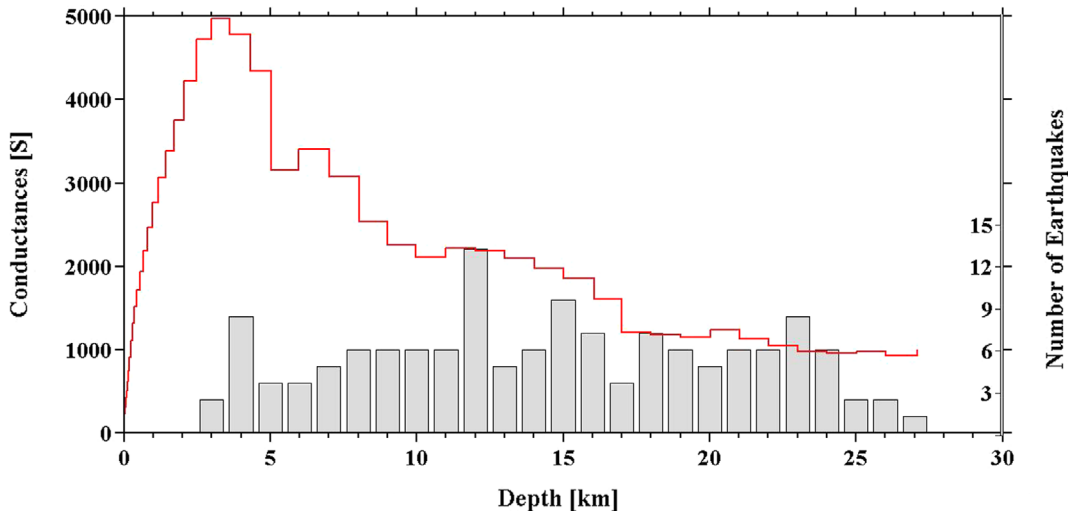

Fig. 4. Conductance of the FZC related to ZFF as a function of depth (red line). It peaks between 2.5–3 km depths. The blue dots show the distribution of earthquakes within 100 km of the MT profile. Note the spatial separation between depths of high fault zone conductance and high seismicity.

applied the method suggested by Bedrosian et al. (2004) to calculate the conductance (horizontally integrated conductivities) of these regions and compare it to the depth distribution of earthquakes. We integrated the conductance of cells restricted by the lateral boundaries of the conductive zones centered on the major faults (with the high level of seismicity) in the SFB and compared it to the depth distribution of earthquake hypocenters in this region. Numerous seismic events with magnitudes between 2.5 M_W and 7 M_W (Karasozen et al., 2019) were considered. Figure 4 shows the result for the FZC close to the ZFF (the results for the FZCs associated to the KZ and KB faults are presented as Figs. S13 and S14 in the electronic supplementary material). The conductance peaks at 5000 S throughout the FZC of ZFF and can be compared with that around KB fault. In all FZCs the conductance is greatest between depths of 2.5 and 3.0 km. An outstanding feature in Figure 4 is the spatial separation between the depths of the peak FZC conductance and high seismicity. Seismicity begins at the depth where the conductance decreases with increasing depth. The preferred explanation for this scenario is the aqueous fluids for the enhanced conductivities of the FZCs around the faults. Fluid rich regions are usually devoid of seismicity since shear stresses associated with brittle failure could not be maintained in these regions.

An almost concave conductor has also been recovered in the MT image beneath the High Zagros (C2 in Fig. 3). The surface trace of the MZT coincides with a sharp conductivity contrast at the eastern edge of this feature. Aqueous fluids, metallic minerals, grain boundary graphite films and molten rocks are different physical causes that can be suggested for the observed conductor. However, it's unlikely that mineralization is responsible for the conductor C2, since such a large mineral deposit would be expected to produce detectable magnetic and gravity anomalies that are not observed (Abedi et al., 2018). Furthermore, graphite films could not remain connected in crystalline basement rocks documented for Zagros (Hatzfeld et al., 2003; Talebian and Jackson, 2004) and cause an effective conductor. There is also no geological or geophysical evidence for molten rocks in mid-crustal depths of High Zagros. There is no volcanic field in this region and Plio-Quaternary volcanism is widespread across eastern and central part of Iran close to the zones of presently active faulting, for instance Dasht e Lut desert and Makran mountains (Walker et al., 2009). Fluids generated from dehydration reactions within the subducting Arabian plate are the only candidate that maybe considered as the hydrological implication for the High Zagros conductor. This assumption entails the saline fluids at hydrostatic pressures filling the interconnected fractures of the crystalline basement, which inhibit the seismicity in this region. The distinct lack of FZC corresponding to the MZT implies an impermeable fault-seal preventing the cross fault fluid flow transport or a very narrow FZC that cannot be resolved by MT.

4.3. Comparisons with Seismic Velocity and Seismicity Data

A reasonably comprehensive picture of the region is obtained by integrating seismic velocity model and seismicity data with the final MT inversion model.

1D joint inversion of P-wave receiver functions and the surface wave dispersion data at seismological stations along the same profile were juxtaposed to obtain a 2D S-wave velocity model whose lateral variability was constrained by the Bouguer gravity anomaly data (Motaghi et al., 2015).

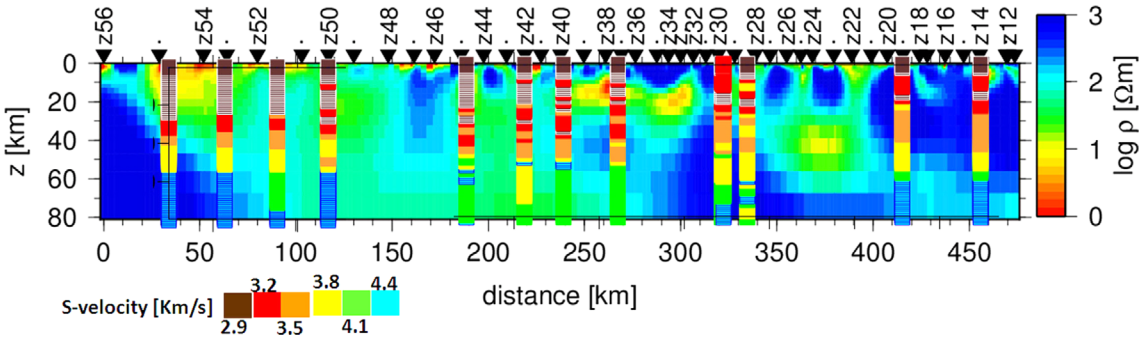

Fig. 5. Electrical resistivity section overlain by S-wave velocity model from Motaghi et al. (2015).

A qualitative comparison between the velocity and resistivity models is presented in Figure 5. Through this integrated interpretation approach, the limitations in sensitivity and resolution of independent geophysical dataset as well as different numerical strategies used to invert these data have to be considered. MT data were inverted using a 2D approach comprised of a minimum smoothness constraint to regularize the inverse problem. However, 2D S-wave velocity model with more continuous low and high-velocity domains (fig. 6 in Motaghi et al., 2015) was obtained by combining 1D absolute S-velocity models of individual stations and smoothing the result with a Gaussian filter width of 30 km.

In general, it seems that domains of low velocities and resistivities beneath the south west of Zagros, are spatially coincident. This is consistent with the known geology of the region, where an upper layer of at least 10 km thickness composed of Cambrian to Miocene sediments overlays the crystalline basement and produces an almost negligible magnetic response (Abedi et al., 2018).

Sparse lateral sampling of MT data (caused by large average site spacing of 15 km) as well as smoothest 2D inversion modeling approach cause the upper crustal conductive layer (C1) to be recovered discontinuous, beneath the SW of the profile. However, coincident seismic studies based on juxtaposed 1D velocity models imaged a more homogenous velocity structure in this region.

We interpolate the coincident and independently derived seismic velocity (Motaghi et al., 2015) and electrical resistivity (Fig. 3) models on to a common grid to obtain a histogram of the correlation between V_S and electrical resistivity in the upper 28.5 km of the Zagros profile. A general increase of electrical resistivity with increasing seismic velocity, representative of decreasing porosity, is apparent (Fig. 6).

Since the histogram grid is very coarse (of 1000 m, limited by the size of the seismic model grid), only three localized zones (I, II and III in Fig. 6) have been chosen. The zones were mapped back into the resistivity section to determine the spatial regions where these zones derive (zones I, II and III in Fig. 3). The region of high resistivity/velocity (zone III) corresponds to the upper crust of central Iran Continental block. The zone (II) is defined

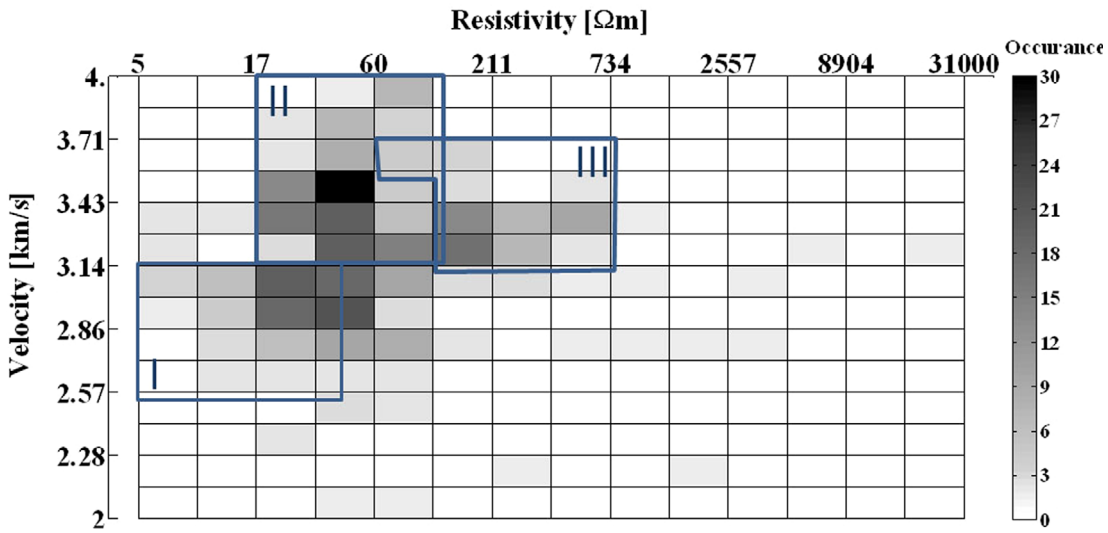

Fig. 6. Quantitative correlation between resistivity and velocity models. A general increasing trend of velocity versus resistivity is apparent in this histogram. Also, three labeled zones of high correlation are presented in this figure.

https://doi.org/10.1007/s12303-020-0024-9

by moderate resistivities and moderate to high velocities and is located beneath the High Zagros and SSZ. The zone (I) has the lowest resistivity/velocity values and coincides with the sedimentary cover of the Arabian crust.

The prominent conductivity contrast beneath the MZT corresponds to steep gradient in both Bouguer gravity and magnetic intensity (Abedi et al., 2018) as well as sharp boundary between low velocities of the ZFTB upper crust and higher velocities beneath SSZ and UDMA (Fig. 5). These concurrent changes in different physical properties provide strong support for a deep seated fault, cross-cutting the whole crust and upper mantle, as estimated by joint interpretation of seismic and gravity data (Motaghi et al., 2015). Although these authors show that a high velocity/density lithosphere beneath Zagros (V_S ~4.8 km/s, $\rho \geq 3.4$), representative of the leading edge of the Arabian shield, is sinking beneath SSZ, UDMA and Central Iran, but this is not confirmed by our resistivity model. Long period MT measurements being able to penetrate deeper levels up to the lithosphere-asthenosphere boundary will be required to constrain more accurately the deep structure beneath Zagros suture zone.

Figure 7 shows the pattern of crustal seismicity occurred within 100 km distance from the MT profile (white dots in Fig. 1) superposed on electrical resistivity section. Earthquake hypocenters are from an updated catalog of 2500 earthquakes (red and white dots in Fig. 1) whose source parameters have been determined from locally and teleseismically recorded earthquakes (Karasozen et al., 2019). The authors used a calibrated earthquake relocation method improved by InSAR data. These seismic hypocentral calibrated locations of earthquakes (referred to as the Global Catalog of Calibrated Earthquake Locations (GCCEL)) are uploaded to the GCCEL catalog (https://www.sciencebase.gov/catalog/item/59fb91fde4b0531197b16ac7).

Towards northeast of the resistive structure recovered beneath the KB fault (R_3), the Zagros mountain belt is nearly devoid of seismicity. Seismicity in Zagros is most pronounced in the SFB. Despite high seismic activity in Zagros belt, no event has been located beneath the MZT region in central Zagros as well as in the SSZ (Paul et al., 2006).

The High Zagros includes NW-striking thrust and reverse faults with notable surface exposure where the most important ones are the MZT and HZF. However, several seismogenic basement thrust faults, without surface rupturing are accommodated beneath the SFB. The main front fault (MFF) and the Zagros Foredeep fault (ZFF) are the two major thrusts in this region. Furthermore, a series of strike slip faults, striking roughly to the N-S direction (KZ, BO, KB, SP and SV faults) are the only major faults scratching the earth surface in this region (Fig. 1).

Thrust faulting is the most frequent earthquake mechanism that usually takes place in the Zagros. The earthquakes mainly occur within the lower parts of the SFB sedimentary cover rather than the HZ (Fig. 7) and are restricted to low elevated regions with an average strike direction along NW-SE azimuth, coincident with the range orientation. They are very rare and usually absent beneath HZ and farther to the north east in the CIMC (Fig. 1). Weak horizons located at the base (the Hormoz evaporite), in the middle and upper parts (e.g., Gurpi Marls, Gachsaran evaporites) of the cover form a regional barrier to vertical rupture propagation and cause moderate size earthquakes with magnitudes $M_W \leq 6.1$ to be the typical seismicity of the SFB (Nissen et al., 2011).

The intense deformation within the ZFTB spans brittle damage elements (minor faults and slip-surface with or without striation) around different faults in this region and maintains a connected network for fluids released into the FZCs. Dehydration reactions within the subducting Arabian plate (in continental crust, mostly due to the amphibolites to granulites metamorphism (Glover and Vine, 1995)), provide a continuous recharge of fluids (Bedrosian, 2007).

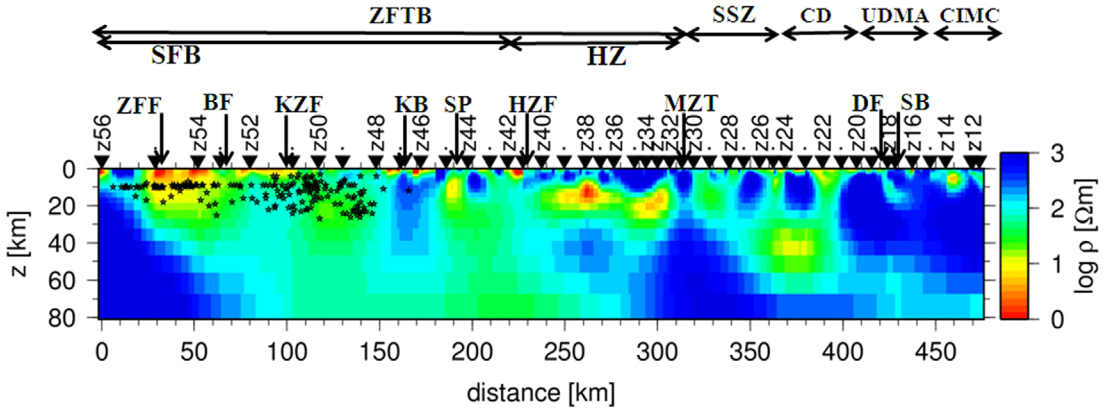

Fig. 7. Seismicity data (black stars) provided by Karasozen et al. (2019) for 100 km strip on either sides of the MT transect (whose epicenters are plotted by the white dots in Fig. 1) are superposed on the electrical resistivity section. Earthquake magnitudes are between (2.5–7) M_W.

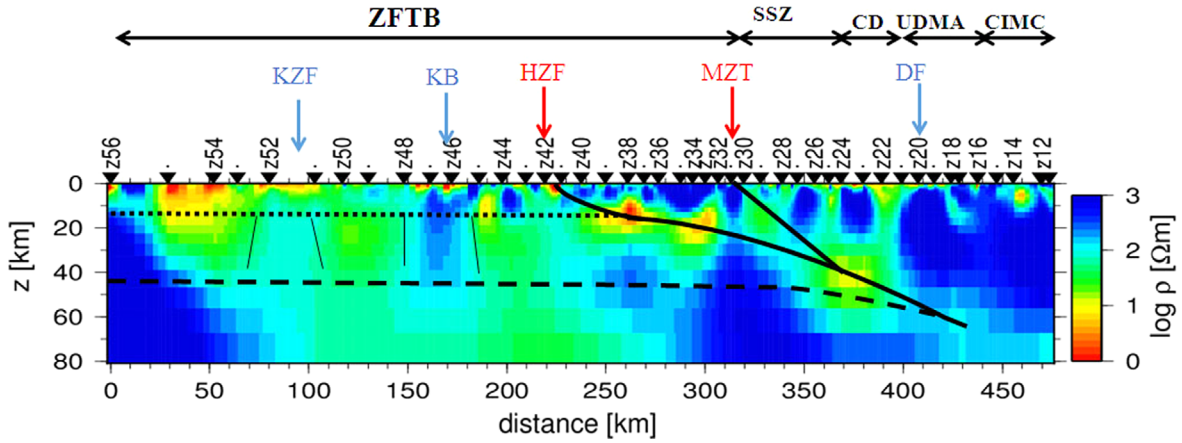

Fig. 8. Geological interpretation of the MT model (see explanation on the text). The main faults cross-cutting the profile, are indicated by the arrows (in red with mainly SW-NE strike and in blue mainly N-S strike). The dotted line indicates the detachment level of folded sedimentary cover (10–15 km thick), corresponding to the Hormuz salt formation. The dashed line indicates Moho, inferred from seismic studies (Paul et al., 2010).

Dashed and dotted lines in Figure 8 represent respectively the Moho discontinuity and the detachment level of the folded sedimentary cover. The Moho depth is inferred from seismic studies (Paul et al., 2010). The detachment level of folded sedimentary corresponds to the Hormuz salt formation. Both, the salt formation and the sedimentary cover on top are imaged as low resistivity structures in the model (between sites z56 and z42) with values lower than 60–70 Ωm.

This detachment level joins the trace of the HZF at depth (black continuous dipping line in Fig. 8). The HZF allows thrusting the sedimentary cover and uploading the older and more resistive rocks (Paleozoic rocks), between sites z42 and z32, with resistivity values more than 500 Ωm. The Arabian crust, between the detachment level and the Moho, contains heterogeneous blocks (as Kazerun Fault (KZF)) probably inherited from Precambrian times. They are imaged as zones of low and high resistivities (marked by short vertical black lines in Fig. 8). The earthquakes are concentrated in a specific seismic zone extended at the basement depths between sites z54 and z46 (see Fig. 7). By contrast, the seismicity is scarce to the NE of the site z45. To explain this feature the resistive structure beneath Karehbas fault, KB, (sites z47–z46) could be considered as a low permeable zone, retaining the fluids released along with the HZF and leading to a more ductile behavior of the crust located to the NE of the KB fault.

Finally, the second black continuous dipping line (in Fig. 8) from MZT represents the contact between Arabian and Iranian plates. On the side of the Iranian plate, the section shows lateral changes in resistivity structure that can be associated to heterogeneous blocks of conductive metamorphic materials beneath the SSZ and the resistive volcanic blocks of oceanic crust (ophiolites) beneath the UDMA.

5. CONCLUSION

An integrated geophysical interpretation along a profile across central Zagros is proposed based upon distortion corrected MT data as well as seismic velocity and seismicity data. Galvanic distortion analysis on MT data results the most accurate 2D impedances in regional coordinate system. The strategy used to reduce 3D effects from 2D inversion of these data, produces a robust geoelectric model whose main features are compatible with the geology and tectonics of this region. Within the SFB of Zagros folded belt to the South west of the KZF, the upper crust is characterized by a zone of low resistivity and velocity extending from surface to depths more than 10 km. This feature is attributed to the thick sedimentary sequence of the Arabian platform. A quantitative correlation between resistivity and velocity models shows a general increasing trend of velocity versus resistivity. Furthermore, three regions of high correlation were determined.

Close to the faults, the possible effects of fluid filled voids and fractures within brecciated and damaged zones of the faults have also been considered. An investigation of the conductance around the major faults in this region shows its decreasing trend with increasing depth. The combination of seismicity data with the conductance values at the FZCs suggests aqueous fluids for the enhanced conductivities. It should be noted that the inferred fluids related to the FZCs is best resolved to be far from the source region of the earthquakes. Thus we propose a scenario for the fluid distribution beneath central Zagros controlling its seismic behavior. However, additional geophysical data including 3D studies of the major faults are essential to further understand the tectonic processes at the Zagros collision belt.

https://doi.org/10.1007/s12303-020-0024-9

ACKNOWLEDGMENTS

We wish to thank Dr. Khalil Motaghi for providing us with the seismic velocity model and Dr. Ezgi Karasözen for seismicity data used in this study. The paper has been greatly improved by the comments of anonymous reviewers.

REFERENCES

Abedi, M., Fournier, D., Devriese, S., and Oldenburg, D.W., 2018, Potential field signatures along the Zagros collision zone in Iran. Tectonophysics, 722, 25–42.

Bedrosian, P., 2007, MT+, integrating magnetotellurics to determine earth structure, physical state, and processes. Surveys in Geophysics, 28, 121–167.

Bedrosian, P., Unsworth, M., Egbert, G., and Thurber, C., 2004, Geophysical images of the creeping San Andreas fault: implications for the role of crustal fluids in the earthquake process. Tectonophysics, 358, 137–158.

Bosak, P., Jaros, J., Spudil, J., Sulovsky, P., and Vaclavek, V., 1998, Salt plugs in the eastern Zagros, Iran: results of regional geological reconnaissance. Geolines, 7, 174.

Caldwell, T.G., Bibby, H.M., and Brown, C., 2004, The magnetotelluric phase tensor. Geophysical Journal International, 158, 457–469.

Chave, A.D. and Jones, A.G., 2012, The Magnetotelluric Method – Theory and Practice. Cambridge University Press, Cambridge, 570 p.

Dehghani, G.A. and Makris, J., 1984, The gravity field and crustal structure of Iran. Neues Jahrbuch für Geologie und Paläontologie, 168, 215–229.

Gabàs, A., Macau, A., Benjumea, B., Queralt, P., Ledo, J., Figueras, S., and Marcuello, A., 2016, Joint audio-magnetotelluric and passive seismic imaging of the Cerdanya Basin. Surveys in Geophysics, 37, 897–921.

García-Yeguas, A., Ledo, J., Piña-Varas, P., Prudencio, J., Queralt, P., Marcuello, A., Ibañez, J.M., Benjumea, B., Sánchez-Alzola, A., and Pérez, N., 2017, A 3D joint interpretation of magnetotelluric and seismic tomographic models: the case of the volcanic island of Tenerife. Computer and Geoscience, 109, 95–105.

Glover, P.W.J. and Vine, F.J., 1995, Beyond KTB-electrical conductivity of the deep continental crust. Surveys in Geophysics, 16, 5–36.

Hatzfeld, D., Tatar, M., Priestley, K., and Ghafory-Ashtyany, M., 2003, Seismological constraints on the crustal structure beneath the Zagros mountain belt (Iran). Geophysical Journal International, 155, 403–410.

Karasözen, E., Nissen, E., Bergman, E.A., and Ghods, A., 2019, Seismotectonics of the Zagros (Iran) from orogen-wide, calibrated earthquake relocations. Journal of Geophysical Research: Solid Earth, 124, 9109–9129.

Khadivi, S., 2010, Tectonic evolution and growth of the Zagros Mountain Belt (Fars, Iran): constraints from magnetostratigraphy, sedimentology and low-temperature thermochronometry. Ph.D. Thesis, Université Pierre et Marie Curie, Paris, 243 p.

Layegh-Haghighi, T., Montahaei, M., and Oskooi, B., 2018, MT data inversion and sensitivity analysis to image electrical structure of Zagros collision zone. Journal of Applied Geophysics, 148, 23–32.

Ledo, J., 2005, 2-D versus 3-D magnetotelluric data interpretation. Surveys in Geophysics, 26, 511–543.

Ledo, J., Queralt, P., Martí, A., and Jones, A.G., 2002, Two-dimensional interpretation of three-dimensional magnetotelluric data: an example of limitations and resolution. Geophysical Journal International, 150, 127–139.

Li, S., Unsworth, M.J., Booker, J.R., Wei, W., Tan, H., and Jones, A.G., 2003, Partial melt or aqueous fluid in the midcrust of Southern Tibet? Constraints from INDEPTH magnetotelluric data. Geophysical Journal International, 153, 289–304.

Manaman, N.S., Shomali, Z.H., and Koyi, H.A., 2011, New constraints on upper-mantle S-velocity structure and crustal thickness of the Iranian plateau using partitioned waveform inversion. Geophysical Journal International, 184, 247–267.

Masson, F., Chéry, J., Hatzfeld, D., Martinod, J., Vernant, P., Tavakoli, F., and Ghafory-Ashtiani, M., 2005, Seismic versus aseismic deformation in Iran inferred from earthquakes and geodetic data. Geophysical Journal International, 160, 217–226.

McNeice, G.W. and Jones, A.G., 2001, Multisite, multifrequency tensor decomposition of magnetotelluric data. Geophysics, 66, 158–173.

Motaghi, K., Shabanian, E., Tatar, M., Cuffaro, M., and Doglioni, C., 2017, The south Zagros suture zone in teleseismic images. Tectonophysics, 694, 292–301.

Motaghi, K., Tatar, M., Priestley, K., Romanelli, F., Doglioni, C., and Panza, G.F., 2015, The deep structure of the Iranian Plateau. Gondwana Research, 28, 407–418.

Nissen, E., Tatar, M., Jackson, J.A., and Allen, M.B., 2011, New views on earthquake faulting in the Zagros fold-and-thrust belt of Iran. Geophysical Journal International, 186, 928–944.

Oskooi, B., Pedersen, L.B., and Koyi, H.A., 2013, Magnetotelluric signature for the Zagros collision. Geophysical Journal International, 196, 1299–1310.

Parker, R.L., 1982, The existence of a region inaccessible to magnetotelluric sounding. Geophysical Journal International, 68, 165–170.

Paul, A., Kaviani, A., Hatzfeld, D., Tatar, M., and Pequegnat, C., 2010, Seismic imaging of the lithospheric structure of the Zagros mountain belt (Iran). In: Leturmy, P. and Robin, C. (eds.), Tectonic and Stratigraphic Evolution of Zagros and Makran during the Mesozoic. Geological Society, London, Special Publications, 330, p. 5–18. https://doi.org/10.1144/SP330.2

Paul, A., Kaviani, A., Hatzfeld, D., Vergne, J., and Mokhtari, M., 2006, Seismological evidence for crustal-scale thrusting in the Zagros mountain belt (Iran). Geophysical Journal International, 166, 227–237.

Pirouz, M., Avouac, J.P., Hassanzadeh, J., Kirschvink, J.L., and Bahroudi, A., 2017, Early Neogene foreland of the Zagros, implications for the initial closure of the Neo-Tethys and kinematics of crustal shortening. Earth and Planetary Science Letters, 477, 168–182.

Ritter, O., Hoffmann-Rothe, A., Bedrosian, P.A., Weckmann, U., and Haak, V., 2005, Electrical conductivity images of active and fossil fault zones. In: Bruhn, D. and Burlini, L. (eds.), High-Strain Zones: Structure and Physical Properties. Geological Society, London, Special Publications, 245, p. 165–186. https://doi.org/10.1144/GSL.SP.2005.245.01.08

Rodi, W. and Mackie, R.L., 2001, Nonlinear conjugate gradients algorithm for 2-D magnetotelluric inversions. Geophysics, 66, 174–187.

Sherkati, S., Letouzey, J., and Frizon de Lamotte, D., 2006, Central Zagros fold-thrust belt (Iran): new insights from seismic data, field observation, and sandbox modeling. Tectonics, 25. https://doi.org/10.1029/2004TC001766

Snyder, D.B. and Barazangi, M., 1986, Deep crustal structure and flexure of the Arabian plate beneath the Zagros collisional mountain belt as inferred from gravity observations. Tectonics, 5, 361–373.

Talebian, M. and Jackson, J., 2004, A reappraisal of earthquake focal mechanisms and active shortening in the Zagros mountains of Iran. Geophysical Journal International, 156, 506–526.

Unsworth, M.J., 2010, Magnetotelluric studies of active continent-continent collisions. Surveys in Geophysics, 31, 137–161.

Walker, R.T., Gans, P., Allen, M.B., Jackson, J., Khatib, M., Marsh, N., and Zarrinkoub, M., 2009, Late Cenozoic volcanism and rates of active faulting in eastern Iran. Geophysical Journal International, 177, 783–805.

Wannamaker, P.E., Caldwell, T.G., Jiracek, G.R., Maris, V., Hill, G.J., Ogawa, Y., Bibby, H.M., Bennie, S.L., and Heise, W., 2009, Fluid and deformation regime of an advancing subduction system at Marlborough, New Zealand. Nature, 460, 733–736.

https://doi.org/10.1007/s12303-020-0024-9